APPLIED SCIENCES AND ENGINEERING

10.1126/sciadv.1501381

High-performance 3D printing of hydrogels by water-dispersible photoinitiator nanoparticles

Amol A. Pawar,[1] Gabriel Saada,[1] Ido Cooperstein,[1] Liraz Larush,[1] Joshua A. Jackman,[2,3] Seyed R. Tabaei,[2,3] Nam-Joon Cho,[2,3] Shlomo Magdassi[1]*

In the absence of water-soluble photoinitiators with high absorbance in the ultraviolet (UV)–visible range, rapid three-dimensional (3D) printing of hydrogels for tissue engineering is challenging. A new approach enabling rapid 3D printing of hydrogels in aqueous solutions is presented on the basis of UV-curable inks containing nanoparticles of highly efficient but water-insoluble photoinitiators. The extinction coefficient of the new water-dispersible nanoparticles of 2,4,6-trimethylbenzoyl-diphenylphosphine oxide (TPO) is more than 300 times larger than the best and most used commercially available water-soluble photoinitiator. The TPO nanoparticles absorb significantly in the range from 385 to 420 nm, making them suitable for use in commercially available, low-cost, light-emitting diode–based 3D printers using digital light processing. The polymerization rate at this range is very fast and enables 3D printing that otherwise is impossible to perform without adding solvents. The TPO nanoparticles were prepared by rapid conversion of volatile microemulsions into water-dispersible powder, a process that can be used for a variety of photoinitiators. Such water-dispersible photoinitiator nanoparticles open many opportunities to enable rapid 3D printing of structures prepared in aqueous solutions while bringing environmental advantages by using low-energy curing systems and avoiding the need for solvents.

INTRODUCTION

Three-dimensional (3D) printing has gained a lot of interest from a variety of fields in recent years (*1*). The most promising application of 3D printing in soft tissue engineering is the fabrication of hydrogel-based scaffolds with predesigned structures and functionality (*2*). Recent developments in 3D printing of hydrogels have focused on the fabrication of tough, self-recoverable, cell-compatible hydrogels whose architecture is conducive to generation of complex tissues (*3*–*6*). Complex 3D hydrogel scaffolds that have a fully interconnected structure with predefined dimensions and porosity are required for effective repair or regeneration of tissues and organs (*7*, *8*). Hydrogel-based scaffolds are of specific interest to tissue engineering because they provide an environment with high water content, enabling high cell encapsulation densities (*9*–*12*). Among the various rapid-prototyping techniques available for 3D printing of hydrogel 3D structures, such as extrusion-based or jetting-based 3D printing, laser-based 3D printing enables high-speed processing of scaffolds with higher resolution [<100 nm with two-photon polymerization; 1 to 30 μm with stereolithography (SLA)] and higher mechanical strength (*9*). SLA 3D printing based on digital light processing (DLP) uses a digital micromirror device to cure a complete 2D layer of ink in one go, enhancing the throughput of the process. Unlike two-photon polymerization, DLP 3D printers enable fabrication of larger build size and faster processing speed at a significantly lower cost of the equipment (*7*, *9*, *13*). In general, processing of hydrogels using SLA-based 3D printing involves an aqueous solution of an oligomer or reactive monomers, photoinitiator (PI), and/or a cross-linking agent (*9*). The PI plays a crucial role in determining the rate of polymerization and, consequently, the resulting properties of the printed object and the time required for 3D fabrication. For fabrication of hydrogels with live cells, mild processing conditions are desirable, such as avoiding heating, stirring, and use of organic solvents or ultraviolet (UV) exposure (*14*). However, in the absence of highly efficient water-soluble PIs, most current protocols for fabricating hydrogels use nonefficient, poorly water-soluble PIs, which require substantial agitation and/or heating or mixing with organic solvents to obtain clear precursor solutions (*15*). Therefore, there is a need for water-compatible PIs that can overcome the above limitations. Here, we present a general, new approach to enabling rapid 3D printing of hydrogels in aqueous solutions based on the conversion of water-insoluble PIs into highly efficient water-dispersible nanoparticles.

Among the limited choices of commercially available, water-soluble PIs, 2-hydroxy-1-[4-(2-hydroxyethoxy) phenyl]-2-methyl-1-propanone [Irgacure 2959 (I2959), Ciba Specialty Chemicals] is the most commonly reported with aqueous photocurable systems (*14*, *16*). Given this compound's limited solubility in water [0.47% (w/w)], dissolving it completely requires substantial agitation and/or heating or mixing with organic solvents. Furthermore, it exhibits low efficiency and slow rate of polymerization upon irradiation with light with wavelengths above 385 nm (*15*, *17*). Alternatively, use of water-insoluble PIs dissolved in organic solvents or their water-soluble derivatives prepared through tedious synthetic procedures is also reported (*15*, *18*–*21*). Direct substitution on the PI often decreases its photoactivity and, consequently, affects the overall efficiency of polymerization (*22*–*24*). For example, synthesized lithium salt of 2,4,6-trimethylbenzoyl-diphenylphosphine oxide (TPO) is reported to absorb weakly in the visible region from 400 to 420 nm (*15*).

Biocompatible riboflavin (vitamin B2) has also been reported as a water-soluble PI. However, it could function only with a costly two-photon polymerization printer that has a very small build size (*25*). In addition, riboflavin as a PI requires a co-initiator (for example, triethanolamine), nitrogen purging (it is highly susceptible to oxygen), and high power input (>244 mW). Comparative studies indicated that riboflavin-triethanolamine mixture exhibits lower photosensitivity

[1]Casali Center of Applied Chemistry, Institute of Chemistry, The Hebrew University of Jerusalem, 91904 Jerusalem, Israel. [2]School of Materials Science and Engineering, Nanyang Technological University, 50 Nanyang Avenue, Singapore 639798, Singapore. [3]School of Chemical and Biomedical Engineering, Nanyang Technological University, 62 Nanyang Drive, Singapore 637459, Singapore.
*Corresponding author. E-mail: magdassi@mail.huji.ac.il

than the commercially available, water-soluble PI I2959 (*25*). Thus, there is an unmet need for highly efficient water-compatible PIs, with high absorbance in the UV-visible range, to enable rapid 3D printing of hydrogels.

Unlike for polymerization in an aqueous medium, there is a large variety of efficient PIs for nonaqueous systems. Among them, TPO has been claimed to be the most efficient PI in initiating the free radical polymerization of various monomers (*26*, *27*). TPO with "aroyl-phosphinoyl chromophore" exhibits a characteristic UV–near-visible absorption around 350 to 380 nm extending up to 420 to 440 nm, with high molar extinction coefficients ($\varepsilon \sim 300$ to 800 M^{-1} cm^{-1}) (*28*). The long wavelength absorption was identified as an $n \rightarrow \pi^*$ transition that is red-shifted because of a moderately strong conjugation between the phosphonyl group and the carbon atom of the adjacent carbonyl group (*29*, *30*). Free radicals generated by TPO react at high rate constants (~0.2 to 6×10^7 mol^{-1} s^{-1}) with compounds having double bonds, such as styrenes, polyesters, and acrylate and vinyl monomers, resulting in fast and thorough in-depth curing/solidification of photocurable systems (*27*, *31*). TPO exhibits good thermal and shelf stability, as well as photobleaching; hence, it is particularly suited for systems requiring no color or odor (*24*, *26*). It exhibits absorption spectra at wavelengths suitable for cell encapsulation (*15*) and for commercially available 3D SLA printers. However, TPO has very low water solubility (3.13 mg $liter^{-1}$ at 25°C) (*32*), and it should be water-compatible for use in aqueous inks.

Therefore, TPO was selected as a model PI that is converted into water-dispersible nanoparticles. The water-dispersible TPO amorphous nanoparticles were formed by spray drying of volatile microemulsions. The PI nanoparticles enabled rapid 3D printing of complex hydrogel structures in water using SLA-based low-cost 3D printers, without any organic solvent. To the best of our knowledge and experience, this process is impossible to perform with presently available PIs and water-soluble monomers.

RESULTS

Formation and characterization of TPO nanoparticles

Drying of volatile microemulsions by spray drying or lyophilization has been recently reported as a simple method for preparing organic drug nanoparticles (*33*, *34*). The resulting nanoparticles of poorly water-soluble compounds were easily dispersed in water to give a clear, stable dispersion (*34*). Furthermore, the addition of a polymer such as polyvinylpyrrolidone (PVP) prevented crystal growth of the organic compounds during dispersion in water. TPO nanoparticles were prepared by a similar approach, while using oil-in-water microemulsions containing TPO at various concentrations (table S1). Free-flowing, dry powders were obtained after spray drying of microemulsions, for all compositions (table S2). Similar powders were also obtained by lyophilization, which is commonly performed in many laboratories and is suitable for the preparation of small quantities of the PI powder (detailed in the Supplementary Materials).

Dispersion of these powders [0.1% (w/w)] in water resulted in clear aqueous dispersions with a bluish tinge. Dynamic light scattering (DLS) measurements showed unimodal particle size distribution with a polydispersity index in the range from 0.02 to 0.2. The mean TPO nanoparticle size ranged from 180 to 350 nm, wherein TPO nanoparticle size increased significantly [$P < 0.001$; one-way analysis of variance (ANOVA) with Holm-Sidak test for pairwise comparisons] with the increase in TPO concentration in the microemulsion (Fig. 1). The particles in powder form were stable for over 85 days while stored at either −20° or 25°C (no change was observed in the mean TPO particle sizes after dispersion in water; details regarding size and concentration effects are presented in the Supplementary Materials; fig. S1). Cryo–transmission electron microscopy (TEM) imaging of a 0.1% (w/w) aqueous dispersion of powder containing 25% (w/w) TPO nanoparticles exhibited particles with a mean diameter of 305 ± 140 nm ($N = 10$; fig. S2).

Dispersing the powders containing 5 to 15% (w/w) TPO at concentrations higher than 1% (w/w) resulted in a clear transparent system. DLS measurements and cryo-TEM imaging did not reveal the presence of particles, indicating that the TPO is most likely solubilized in the presence of the surfactant. To verify that TPO is not simply solubilized in a micellar solution of surfactants, we dispersed the unprocessed TPO in water with the SDS and PVP at concentrations similar to those in a 1% (w/w) aqueous dispersion of the TPO nanoparticles. The mixture was then subjected to either high-speed stirring for 24 hours at room temperature or sonication for 60 min, followed by filtration using a 0.22-μm filter and measurements of the concentration of solubilized TPO with a UV spectrophotometer. About 85 to 87% (w/w) TPO was solubilized in this micellar solution after a long duration of high-speed stirring or sonication. However, TPO nanoparticles were readily dispersed with simple manual shaking for 1 to 2 min, resulting in a clear system. Furthermore, the dispersions of the TPO nanoparticles were stable at room temperature for a prolonged period and therefore can be used for 3D ink formulations (fig. S3).

The resulting particles of TPO were further studied by x-ray diffraction. The particles were amorphous and did not crystallize even after storage for 85 days at 25°C (fig. S4). The retention of the amorphous property of TPO nanoparticles can be attributed to crystallization inhibition by PVP. PVP has been reported to undergo intermolecular interactions by forming hydrogen bonds with the hydrophobic

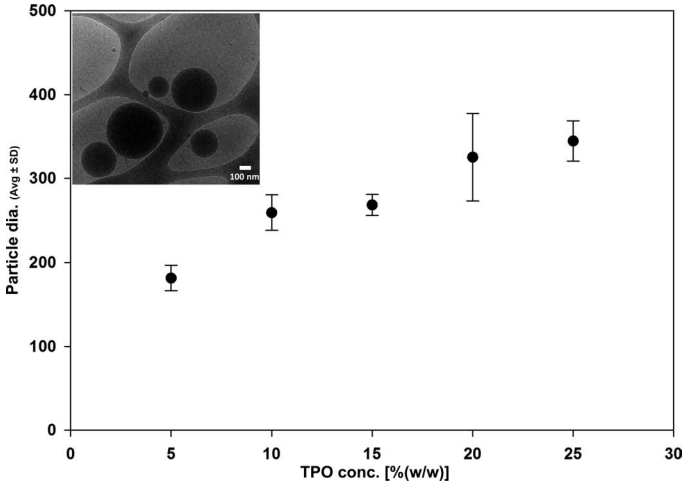

Fig. 1. TPO nanoparticle size. Average (Avg) particle size of an aqueous dispersion of 0.1% (w/w) powder containing TPO nanoparticles obtained from microemulsions with various concentrations of TPO. Inset: Cryo–TEM image of an aqueous dispersion [0.1% (w/w)] of powder containing 25% (w/w) TPO.

compounds and delaying the crystal growth process (*35*) or by increasing the kinetic barrier to nucleation (*36*, *37*).

Efficiency of TPO nanoparticles

Photoinitiation is the most critical step in a photopolymerization process, which determines the kinetics and properties of the resulting polymerized objects. The rate of photopolymerization is generally proportional to the square root of the rate of initiation (R_i) (*15*). For photoinitiated polymerization, R_i is directly proportional to the incident light intensity, the concentration of PI, and the intrinsic properties of the PI. The intrinsic properties of the PI that influence its utility are the molar extinction coefficient (ε), the quantum yield or cleavage events that occur per photon absorbed, and the PI efficiency or the ratio of initiation events to radicals generated by photolysis. For efficient polymerization, the initiator should have a large ε and a good overlapping absorbance spectrum with the emission spectrum of the light sources.

The molar extinction coefficient of TPO nanoparticles was measured and compared with that of the commercial water-soluble PI I2959 using a 4 mM aqueous solution. As shown in Fig. 2, the ε of TPO nanoparticles at 365 nm was ~680 M^{-1} cm^{-1}, more than 300 times larger than that of the most used commercially available water-soluble PI I2959 (ε = 2.25 M^{-1} cm^{-1}). In addition, the TPO nanoparticles absorb significantly in the visible region from 400 to 420 nm, making them suitable also for polymerization on the basis of light-emitting diode (LED) lamps used in DLP-based 3D printing (tables S3 and S4).

The TPO nanoparticles are also superior to another approach to making TPO compatible with water, by chemical modification. Recently, a water-soluble lithium salt of TPO was synthesized and evaluated for its ability to polymerize polyethylene glycol monomers into hydrogels (*15*). The ε of this water-soluble TPO salt was 218 M^{-1} cm^{-1} at 365 nm, which was less than the reported ε of TPO in the organic medium methyl methacrylate (ε_{max} ~ 520 M^{-1} cm^{-1} at 381 nm) (*38*). In comparison with both the reported molar extinction coefficients of lithium salt of TPO in water and unprocessed TPO in organic solvent, the TPO nanoparticles exhibited larger values at the wavelengths of commonly available UV lamps. Up to 3% (w/w) TPO nanoparticles can be dispersed in water at 25°C (100 times more than the water solubility of bulk TPO), without a significant increase in viscosity. Overall, the high water dispersibility and very high molar extinction coefficients at the UV range make the TPO nanoparticles excellent candidates for 3D printing in aqueous solutions, as will be shown in the following polymerization and printing results.

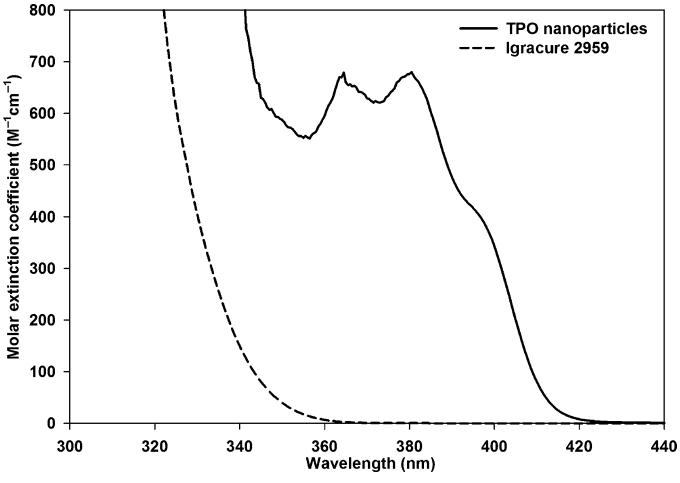

Fig. 2. Molar extinction coefficient of TPO nanoparticles. Molar extinction coefficients of the TPO nanoparticles (solid line) and I2959 (dashed line) obtained by measuring the absorbance of 4 mM aqueous solutions.

Polymerization kinetics of acrylamide in aqueous solutions with TPO nanoparticles was compared to that in aqueous solutions of the commonly used PI I2959 to determine the polymerization efficiency of TPO nanoparticles. A Fourier transform infrared spectrophotometer (ALPHA FT-IR Spectrometer, Bruker) was used in conjunction with a platinum attenuated total reflection (ATR) single-reflection diamond accessory (sample scans, 64; resolution, 4 cm^{-1}). The polymerization medium comprised aqueous solutions of 20% (w/w) monomer (acrylamide) with the cross-linking monomer polyethylene glycol 600 diacrylate [5% (w/w) monomer] and PI [TPO nanoparticles or I2959 at a concentration of 0.5% (w/w) monomer]. The resulting aqueous acrylamide solutions had 2.9 mM TPO and 4.5 mM I2959. Measurements were performed on ~200 μl of a polymerization solution dropped on the ATR diamond. The UV light was radiated onto the sample through a chamber (at 1.5-cm height) centered at the ATR diamond. Monochromatic UV LED (Integration Technology) irradiating at 395 nm was used for photocuring. Infrared spectra were recorded after every 4 s, for a total duration of 40 s. The polymerization kinetics was studied by monitoring the Fourier transform infrared spectra in the range from 1800 to 800 cm^{-1}.

The percentage of conversion of acrylamide was calculated from the decay/disappearance of the absorption peaks of methylene group vibrations at 988 cm^{-1} (assigned to the out-of-plane bending mode of the =C–H unit) normalized to the C=O stretching peak at 1654 cm^{-1} as an internal standard (*39*). The area under the peak at 988 cm^{-1} at different durations of UV exposure was compared with the sample with no UV exposure. As shown in Fig. 3, the TPO nanoparticles enabled much faster photopolymerization of acrylamide than did I2959. With TPO nanoparticles, after ~40 s of irradiation, the =C–H bond peaks disappeared completely (fig. S5A), and the sample on the ATR diamond was completely solidified. However, in the case of solutions with I2959, even after curing for 300 s there was no significant change in =C–H bond peaks (fig. S5B), whereas the sample on the ATR diamond remained in liquid form. As expected, better polymerization profiles were obtained using TPO nanoparticles concordant with the much larger extinction coefficient of the TPO nanoparticles compared to I2959. The measured efficiency of TPO nanoparticles in photopolymerizing aqueous solutions of acrylamide in air at 25°C was found to be highest among various water-compatible PIs reported in the literature (see comparison in table S5).

Three-dimensional printing of hydrogel model using TPO nanoparticles

The suitability of TPO nanoparticles for enabling photopolymerization in water was important in the 3D printing of aqueous acrylamide formulation. The aqueous ink solutions contained 38.5% (w/w) acrylamide with a cross-linking monomer [ethoxylated trimethylolpropane triacrylate, SR-9035; 8.9% (w/w) monomer], PI [TPO nanoparticles or I2959 at a concentration of 2.4% (w/w) monomer], and yellow dye (2.4% of the monomer; Duasyn Acid Yellow XX-SF liquid, Clariant). A predesigned hydrogel model was 3D printed using an

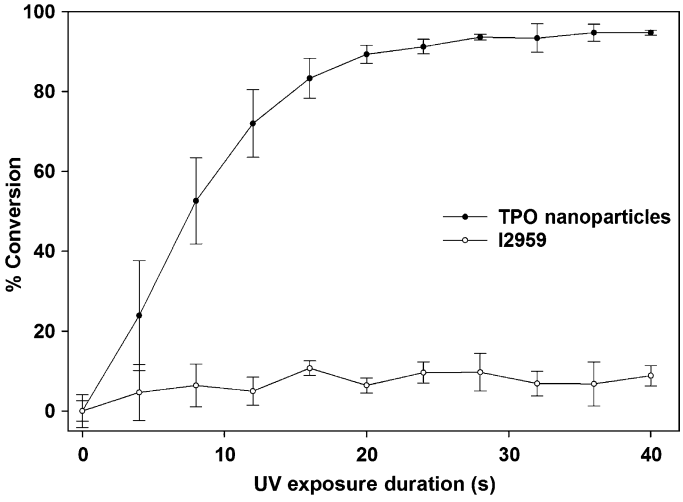

Fig. 3. Polymerization kinetics. Percentage of conversion of vinyl bonds calculated using aqueous acrylamide solutions with TPO nanoparticles and I2959 at 988 cm^{-1} (assigned to the out-of-plane bending mode of the =C–H unit) normalized to the C=O stretching peak at 1654 cm^{-1} as an internal standard at varying durations of UV (395-nm) exposure.

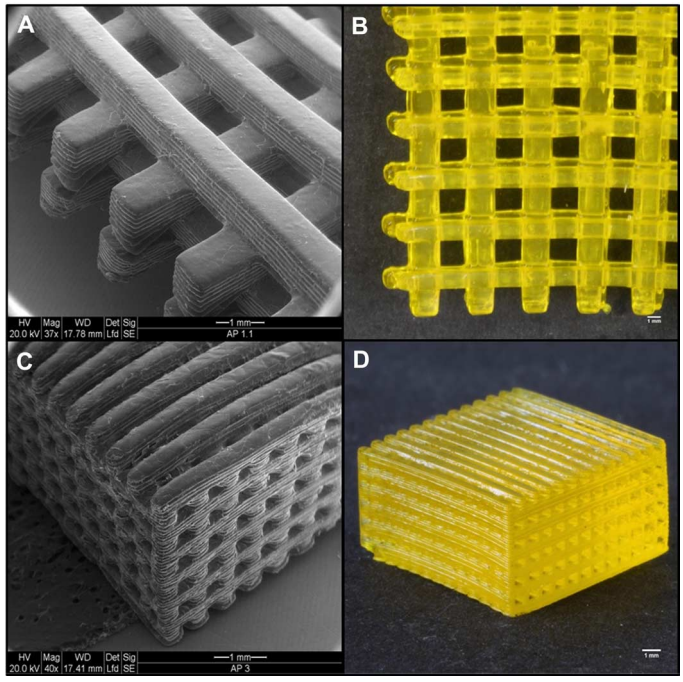

Fig. 4. Three-dimensionally printed hydrogel. (**A** to **D**) Three-dimensionally printed woodpile-structured hydrogel scaffold using TPO nanoparticles.

SLA 3D printer (Freeform Plus 39, Asiga). This printer operates by a top-down SLA system with a digital mirror device and a UV-LED light source (385 nm). After 3D printing, the structures were rinsed with water in a sonicator bath for 1 min to remove the monomer/PI residues. The structures were observed under an environmental scanning electron microscope (Quanta 200 FEG, FEI).

Three-dimensional printing of hydrogel was performed at a rate of 6 s per layer (100-μm layer thickness with 6-s irradiation to each layer). A stable woodpile-structured hydrogel (build size, 25 mm × 25 mm × 3 mm) (Fig. 4) was built within 25 min using TPO nanoparticles. The printed hydrogels had more than 80% (w/w) water content, as detailed in the Supplementary Materials. Cytotoxicity and cell viability studies indicated that the PI nanoparticles and 3D printed hydrogels were biocompatible and comparable to those observed in the commonly used polyethylene glycol diacrylate (PEG-DA) hydrogel scaffold. Experimental details and results regarding biocompatibility studies are presented in the Supplementary Materials. The measured mechanical strength of the printed hydrogels (complex shear modulus, 47.3 ± 0.7 kPa) was more than six times greater than that of the reference PEG-DA hydrogels, indicating that it would likely be strong enough to hold its own weight for in situ and implant purposes. The experimental details are presented in the Supplementary Materials, along with shear storage modulus and shear loss modulus results in fig. S8.

The hydrogel structure obtained from polymerizing aqueous solutions with TPO nanoparticles was compared with that obtained from solutions with I2959 to investigate the differences in photoreactivity and 3D printing capabilities. In contrast to inks containing TPO nanoparticles, no 3D structures could be printed using I2959 aqueous solutions. Even after increasing the curing time per layer (1.5 min per layer) and the concentration of I2959 [up to 20% (w/w) monomer], no hydrogel structure was obtained. The fast polymerization with TPO nanoparticles can be explained in terms of better solubility of the TPO, resulting in improved dispersion and thus fast availability of free monomers to the newly formed free radicals (*24*). Because no chemical modification of PI was involved during the processing of TPO nanoparticles, the characteristic high extinction coefficient of TPO was retained in the aqueous system. Thus, on the basis of these findings, the common and efficient PIs for organic solvent–based inks can be used now for 3D printing of aqueous systems, if converted into nanoparticles. Recent advances in 3D printing involve smart materials that can undergo programmed changes in structure, size, and pattern over the fourth dimension, that is, postprinting time under the influence of external stimuli (*40*). Application of such printing to the biomedical field is defined as 4D bioprinting (*41*). We expect that the new water-dispersible PI nanoparticles could also be used in 4D bioprinting, particularly when water-soluble, stimuli-responsive materials or high water content is a requisite.

CONCLUSION

In summary, preparation of TPO nanoparticles for 3D printing of hydrogels addresses the challenge of having highly efficient water-soluble/water-dispersible PIs with high absorbance in the UV-visible region. We characterized TPO nanoparticles for their effectiveness in initiating polymerizations by 3D printing of a predesigned hydrogel model and fabricated a hydrogel scaffold with high-resolution woodpile structure using an SLA-based 3D printer. Neither chemical modification of PI nor addition of organic solvents was required for obtaining the efficient PI. The presented approach for converting water-insoluble PIs into those that can be used in aqueous systems opens the way for obtaining other PIs and for improving polymerizable aqueous inks for the emerging field of 3D printing.

MATERIALS AND METHODS

Details of Materials and Methods are available in the Supplementary Materials.

Materials

Chemicals were purchased from Sigma and PI was obtained from BASF, unless otherwise specified. Oligomers and cross-linkers were acquired from Sartomer-Arkema. Ultrapure water obtained from NANOpure-DIamond [triple distilled water (TDW)] was used in all of the experiments.

Preparation of PI containing microemulsions

Our previously reported method for preparing nanoparticles of a poorly water-soluble compound by evaporation of volatile oil-in-water microemulsions was used to prepare the PI nanoparticles (*33*). Oil-in-water microemulsions containing varying concentrations of TPO were prepared at room temperature by mixing *n*-butyl acetate with SDS (as surfactant), isopropyl alcohol (as cosolvent), and PVP (as crystallization inhibitor) to create an "oil" (organic) phase in which TPO is dissolved. Afterward, the oil phase was mixed with TDW and magnetically stirred at 25°C until clear systems were obtained. The compositions of microemulsions are presented in table S1.

Conversion of microemulsions into nanoparticles

The above microemulsions were spray-dried by a Mini Spray Dryer B-290 equipped with Inert Loop B-295 and Dehumidifier B-296 (Buchi). The resultant products were dry, free-flowing powders (compositions given in table S2), which were stored in tightly closed glass vials.

Dispersion of TPO nanoparticles in water

The powders obtained at the end of the spray-drying process were dispersed [0.1 to 1% (w/w)] in TDW. The samples were vortexed for 1 min and magnetically stirred at room temperature for 5 min. This powder-dispersing procedure was performed to have a reproducible procedure, although simple manual shaking of the dispersion for 1 to 2 min was sufficient to obtain a clear system.

Size measurements of TPO nanoparticles

The particle size distribution after dispersion in water was measured at room temperature by DLS using a Nano ZS Zetasizer (Malvern).

Cryo-TEM

After dispersing the powder in water [0.1 to 1% (w/w)], the TPO nanoparticles were evaluated by cryo-TEM. All samples were studied under low-dose conditions by an FEI Tecnai 12 G2 transmission electron microscope operated at 120 kV. Images were recorded on a 4K × 4K FEI Eagle charge-coupled device camera.

Crystallinity measurement of TPO nanoparticles

Powder x-ray diffraction (PXRD) measurements were performed using a D8 Advance diffractometer (Bruker AXS).

UV absorption measurements

To evaluate the suitability of the TPO nanoparticles for aqueous ink formulations, we further studied the stability of the aqueous dispersion that was quantified by UV spectroscopy. The stability of dispersed PI nanoparticles in water was evaluated by measuring the TPO concentration in the filtrate at various time intervals after dispersing the powders in water. PI nanoparticles were dispersed in water and subsequently filtered through 0.22-μm polyvinylidene difluoride (PVDF) filters. Quantification of TPO concentration in the filtrate was performed with a UV spectrophotometer (UV-1800, Shimadzu). The experiments indicated that the dispersion remains stable for at least 50 days (fig. S3) and therefore can be used for ink formulations. The molar extinction coefficients (ε) were measured and compared with those of commercially available PI I2959. Absorption spectra were determined in the range from 300 to 440 nm because this range reflects the emission of most commercially available UV lamps.

Measurement of PI activity

To determine the polymerization efficiency of TPO nanoparticles, we measured the polymerization kinetics of acrylamide in aqueous solutions with TPO nanoparticles and compared it to that in aqueous solutions of the commercial water-soluble PI I2959. A Fourier transform infrared spectrophotometer (ALPHA FT-IR Spectrometer, Bruker) was used in conjunction with platinum ATR single-reflection diamond accessory (sample scans, 64; resolution, 4 cm^{-1}). The polymerization solutions comprised aqueous solutions containing 20% (w/w) monomer (acrylamide) with the cross-linking monomer polyethylene glycol 600 diacrylate [5% (w/w) monomer] and PI [TPO nanoparticles or I2959 at a concentration of 0.5% (w/w) monomer].

Three-dimensional printing of model structure

Three-dimensional hydrogels were prepared by UV-curing aqueous solutions containing 38.5% (w/w) monomer (acrylamide) with a cross-linking monomer [ethoxylated trimethylolpropane triacrylate, SR-9035; 8.9% (w/w) monomer], PI [TPO nanoparticles or I2959 at a concentration of 2.4% (w/w) monomer], and yellow dye (2.4% of the monomer; Duasyn Acid Yellow XX-SF liquid, Clariant). A predesigned hydrogel model was 3D printed using an SLA 3D printer (Freeform Plus 39, Asiga). This printer operates by a top-down SLA system with a digital mirror device and a UV-LED light source (385 nm). After 3D printing, the structures were rinsed with water in a sonicator bath for 1 min to remove the monomer/PI residues. The structures were observed under an environmental scanning electron microscope (Quanta 200 FEG, FEI).

SUPPLEMENTARY MATERIALS

Supplementary material for this article is available at http://advances.sciencemag.org/cgi/content/full/2/4/e1501381/DC1

Supplementary Materials and Methods

Biocompatible studies with PI nanoparticles and 3D printed hydrogels.

Determination of 3D printed hydrogel water content.

Determination of 3D printed hydrogel mechanical strength.

Fig. S1. Effect of storage temperature and duration on size of TPO nanoparticles.

Fig. S2. Cryo-TEM image of an aqueous dispersion [0.1% (w/w)] of powder containing 25% (w/w) TPO.

Fig. S3. Stability of TPO in an aqueous dispersion [1.6% (w/w)] of spray-dried powder at different time intervals after filtration through 0.22-μm PVDF filters.

Fig. S4. X-ray diffraction patterns for spray-dried powders containing TPO nanoparticles after 85 days of storage at 25°C.

Fig. S5. Polymerization kinetics.

Fig. S6. Effects of TPO nanoparticle concentration on cell viability.

Fig. S7. Relative cell viability of Huh7 liver cells cultured on different substrates.

Fig. S8. Mechanical characterization of polyacrylamide hydrogel fabricated with TPO nanoparticles.

Table S1. Composition [% (w/w)] of the microemulsions before spray drying.

Table S2. Theoretical composition [in % (w/w)] of the spray-dried powders.

Table S3. Molar extinction coefficients of TPO nanoparticles and I2959 at standard center wavelengths of light sources used for DLP-based 3D printers.

Table S4. Summary of different light sources used for hydrogel formation.
Table S5. Summary of photopolymerization results using different water-soluble PIs with aqueous acrylamide solutions in air at 25°C.
References (*42*–*64*)

REFERENCES AND NOTES

1. J. R. Tumbleston, D. Shirvanyants, N. Ermoshkin, R. Janusziewicz, A. R. Johnson, D. Kelly, K. Chen, R. Pinschmidt, J. P. Rolland, A. Ermoshkin, E. T. Samulski, J. M. DeSimone, Continuous liquid interface production of 3D objects. *Science* **347**, 1349–1352 (2015).
2. S. Wang, J. M. Lee, W. Y. Yeong, Smart hydrogels for 3D bioprinting. *Int. J. Bioprint.* **1**, 3 (2015).
3. S. Hong, D. Sycks, H. F. Chan, S. Lin, G. P. Lopez, F. Guilak, K. W. Leong, X. Zhao, 3D printing of highly stretchable and tough hydrogels into complex, cellularized structures. *Adv. Mater.* **27**, 4035–4040 (2015).
4. A. L. Rutz, K. E. Hyland, A. E. Jakus, W. R. Burghardt, R. N. Shah, A multimaterial bioink method for 3D printing tunable, cell-compatible hydrogels. *Adv. Mater.* **27**, 1607–1614 (2015).
5. J. Wei, J. Wang, S. Su, S. Wang, J. Qiu, Z. Zhang, G. Christopher, F. Ning, W. Cong, 3D printing of an extremely tough hydrogel. *RSC Adv.* **5**, 81324–81329 (2015).
6. C. B. Highley, C. B. Rodell, J. A. Burdick, Direct 3D printing of shear-thinning hydrogels into self-healing hydrogels. *Adv. Mater.* **27**, 5075–5079 (2015).
7. S. V. Murphy, A. Atala, 3D bioprinting of tissues and organs. *Nat. Biotechnol.* **32**, 773–785 (2014).
8. F. P. W. Melchels, X. Qu, W. Zhu, M. Xiang, J. Yang, K. Zhang, Y. Wei, S. Chen, Additive manufacturing of tissues and organs. *Prog. Polym. Sci.* **37**, 1079–1104 (2012).
9. T. Billiet, M. Vandenhaute, J. Schelfhout, S. Van Vlierberghe, P. Dubruel, A review of trends and limitations in hydrogel-rapid prototyping for tissue engineering. *Biomaterials* **33**, 6020–6041 (2012).
10. M. Gou, X. Qu, W. Zhu, M. Xiang, J. Yang, K. Zhang, Y. Wei, S. Chen, Bio-inspired detoxification using 3D-printed hydrogel nanocomposites. *Nat. Commun.* **5**, 3774 (2014).
11. T. Q. Huang, X. Qu, J. Liu, S. Chen, 3D printing of biomimetic microstructures for cancer cell migration. *Biomed. Microdevices* **16**, 127–132 (2014).
12. X. Li, R. Cui, L. Sun, K. E. Aifantis, Y. Fan, Q. Feng, F. Cui, F. Watari, 3D-printed biopolymers for tissue engineering application. *Int. J. Polym. Sci.* **2014**, 829145 (2014).
13. J. Malda, J. Visser, F. P. Melchels, T. Jüngst, W. E. Hennink, W. J. A. Dhert, J. Groll, D. W. Hutmacher, 25th anniversary article: Engineering hydrogels for biofabrication. *Adv. Mater.* **25**, 5011–5028 (2013).
14. C. G. Williams, A. N. Malik, T. K. Kim, P. N. Manson, J. H. Elisseeff, Variable cytocompatibility of six cell lines with photoinitiators used for polymerizing hydrogels and cell encapsulation. *Biomaterials* **26**, 1211–1218 (2005).
15. B. D. Fairbanks, M. P. Schwartz, C. N. Bowman, K. S. Anseth, Photoinitiated polymerization of PEG-diacrylate with lithium phenyl-2,4,6-trimethylbenzoylphosphinate: Polymerization rate and cytocompatibility. *Biomaterials* **30**, 6702–6707 (2009).
16. S. J. Bryant, C. R. Nuttelman, K. S. Anseth, Cytocompatibility of UV and visible light photoinitiating systems on cultured NIH/3T3 fibroblasts in vitro. *J. Biomater. Sci. Polym. Ed.* **11**, 439–457 (2000).
17. H. Lin, D. Zhang, P. G. Alexander, G. Yang, J. Tan, A. W.-M. Cheng, R. S. Tuan, Application of visible light-based projection stereolithography for live cell-scaffold fabrication with designed architecture. *Biomaterials* **34**, 331–339 (2013).
18. S. Park, D. Kim, S. Y. Ko, J.-O. Park, S. Akella, B. Xu, Y. Zhang, S. Fraden, Controlling uniformity of photopolymerized microscopic hydrogels. *Lab Chip* **14**, 1551–1563 (2014).
19. J. Qiu, J. Wei, Water-soluble and polymerizable thioxanthone photoinitiator containing imidazole. *J. Appl. Polym. Sci.* **131**, 40659 (2014).
20. J. Zhang, F. Dumur, P. Xiao, B. Graff, D. Bardelang, D. Gigmes, J. Pierre Fouassier, J. Lalevée, Structure design of naphthalimide derivatives: Toward versatile photoinitiators for near-UV/visible LEDs, 3D printing, and water-soluble photoinitiating systems. *Macromolecules* **48**, 2054–2063 (2015).
21. K. Kojima, M. Ito, H. Morishita, N. Hayashi, A novel water-soluble photoinitiator for the acrylic photopolymerization type resist system. *Chem. Mater.* **10**, 3429–3433 (1998).
22. Y. Yagci, S. Jockusch, N. J. Turro, Photoinitiated polymerization: Advances, challenges, and opportunities. *Macromolecules* **43**, 6245–6260 (2010).
23. R. Guo, Y. Gao, M. Wu, H. Wang, Aliphatic ketones and aldehydes as water-soluble photoinitiators for the photopolymerization of methacrylic acid. *Polymer* **54**, 4940–4947 (2013).
24. V. Castelvetro, M. Molesti, P. Rolla, UV-curing of acrylic formulations by means of polymeric photoinitiators with the active 2,6-dimethylbenzoylphosphine oxide moieties pendant from a tetramethylene side chain. *Macromol. Chem. Phys.* **203**, 1486–1496 (2002).
25. A. K. Nguyen, S. D. Gittard, A. Koroleva, S. Schlie, A. Gaidukeviciute, B. N. Chichkov, R. J. Narayan, Two-photon polymerization of polyethylene glycol diacrylate scaffolds with riboflavin and triethanolamine used as a water-soluble photoinitiator. *Regen. Med.* **8**, 725–738 (2013).
26. H. F. Gruber, Photoinitiators for free-radical polymerization. *Prog. Polym. Sci.* **17**, 953–1044 (1992).
27. T. Sumiyoshi, W. Schnabel, A. Henne, P. Lechtken, On the photolysis of acylphosphine oxides. 1. Laser flash-photolysis studies with 2,4,6-trimethylbenzoyldiphenylphosphine oxide. *Polymer* **26**, 141–146 (1985).
28. U. Kolczak, G. Rist, K. Dietliker, J. Wirz, Reaction mechanism of monoacyl- and bisacylphosphine oxide photoinitiators studied by ^{31}P-, ^{13}C-, and ^{1}H-CIDNP and ESR. *J. Am. Chem. Soc.* **118**, 6477–6489 (1996).
29. M. Spichty, N. J. Turro, G. Rist, J.-L. Birbaum, K. Dietliker, J.-P. Wolf, G. Gescheidt, Bond cleavage in the excited state of acyl phosphene oxides: Insight on the role of conformation by model calculations: A concept. *J. Photochem. Photobiol. A Chem.* **142**, 209–213 (2001).
30. S. Jockusch, N. J. Turro, Phosphinoyl radicals: Structure and reactivity. A laser flash photolysis and time-resolved ESR investigation. *J. Am. Chem. Soc.* **120**, 11773–11777 (1998).
31. R. S. Davidson, The chemistry of photoinitiators—Some recent developments. *J. Photochem. Photobiol. A Chem.* **73**, 81–96 (1993).
32. Committee for Risk Assessment, Background document to the Opinion proposing harmonised classification and labelling at Community level of diphenyl(2,4,6-trimethylbenzoyl)phosphine oxide, ECHA/RAC/CLH-O-0000001405-81-01/A1 (European Chemical Agency, Dortmund, Germany, 2010), p. 6.
33. K. Margulis-Goshen, S. Magdassi, Formation of simvastatin nanoparticles from microemulsion. *Nanomedicine* **5**, 274–281 (2009).
34. K. Margulis-Goshen, H. D. Netivi, D. T. Major, M. Gradzielski, U. Raviv, S. Magdassi, Formation of organic nanoparticles from volatile microemulsions. *J. Colloid Interface Sci.* **342**, 283–292 (2010).
35. G. A. Ilevbare, H. Liu, K. J. Edgar, L. S. Taylor, Maintaining supersaturation in aqueous drug solutions: Impact of different polymers on induction times. *Cryst. Growth Des.* **13**, 740–751 (2013).
36. U. S. Kestur, H. Lee, D. Santiago, C. Rinaldi, Y.-Y. Won, L. S. Taylor, Effects of the molecular weight and concentration of polymer additives, and temperature on the melt crystallization kinetics of a small drug molecule. *Cryst. Growth Des.* **10**, 3585–3595 (2010).
37. H. Konno, L. S. Taylor, Influence of different polymers on the crystallization tendency of molecularly dispersed amorphous felodipine. *J. Pharm. Sci.* **95**, 2692–2705 (2006).
38. M. G. Neumann, W. G. Miranda Jr., C. C. Schmitt, F. A. Rueggeberg, I. C. Correa, Molar extinction coefficients and the photon absorption efficiency of dental photoinitiators and light curing units. *J. Dent.* **33**, 525–532 (2005).
39. S. C. Kang, Y. J. Choi, H. Z. Kim, J. B. Kyong, D. K. Kim, Kinetics of acrylamide solution polymerization using potassium persulfate as an initiator by in situ IR. *Macromol. Res.* **12**, 107–111 (2004).
40. Z. X. Khoo, J. E. M. Teoh, Y. Liu, C. K. Chua, S. Yang, J. An, K. F. Leong, W. Y. Yeong, 3D printing of smart materials: A review on recent progresses in 4D printing. *Virtual Phys. Prototyp.* **10**, 103–122 (2015).
41. J. An, C. K. Chua, V. Mironov, A perspective on 4D bioprinting. *Int. J. Bioprinting* **2**, 3–5 (2015).
42. A. Ovsianikov, A. Deiwick, S. Van Vlierberghe, P. Dubruel, L. Möller, G. Dräger, B. Chichkov, Laser fabrication of three-dimensional CAD scaffolds from photosensitive gelatin for applications in tissue engineering. *Biomacromolecules* **12**, 851–858 (2011).
43. D. Dyondi, T. J. Webster, R. Banerjee, A nanoparticulate injectable hydrogel as a tissue engineering scaffold for multiple growth factor delivery for bone regeneration. *Int. J. Nanomed.* **8**, 47–59 (2013).
44. L. G. Vincent, Y. S. Choi, B. Alonso-Latorre, J. C. del Álamo, A. J. Engler, Mesenchymal stem cell durotaxis depends on substrate stiffness gradient strength. *Biotechnol. J.* **8**, 472–484 (2013).
45. K. Arcaute, B. Mann, R. Wicker, Stereolithography of spatially controlled multi-material bioactive poly(ethylene glycol) scaffolds. *Acta Biomater.* **6**, 1047–1054 (2010).
46. M. Kurečič, M. Sfiligoj-Smole, K. Stana-Kleinschek, UV polymerization of poly (*N*-isopropylacrylamide) hydrogel. *Mater. Technol.* **46**, 87–91 (2012).
47. V. L. Tsang, A. A. Chen, L. M. Cho, K. D. Jadin, R. L. Sah, S. DeLong, J. L. West, S. N. Bhatia, Fabrication of 3D hepatic tissues by additive photopatterning of cellular hydrogels. *FASEB J.* **21**, 790–801 (2007).
48. A. Khademhosseini, R. Langer, Microengineered hydrogels for tissue engineering. *Biomaterials* **28**, 5087–5092 (2007).
49. T. Billiet, E. Gevaert, T. De Schryver, M. Cornelissen, P. Dubruel, The 3D printing of gelatin methacrylamide cell-laden tissue-engineered constructs with high cell viability. *Biomaterials* **35**, 49–62 (2014).
50. L. A. Hockaday, K. H. Kang, N. W. Colangelo, P. Y. C. Cheung, B. Duan, E. Malone, J. Wu, L. N. Girardi, L. J. Bonassar, H. Lipson, C. C. Chu, J. T. Butcher, Rapid 3D printing of anatomically accurate and mechanically heterogeneous aortic valve hydrogel scaffolds. *Biofabrication* **4**, 035005 (2012).
51. R. Gauvin, Y.-C. Chen, J. W. Lee, P. Soman, P. Zorlutuna, J. W. Nichol, H. Bae, S. Chen, A. Khademhosseini, Microfabrication of complex porous tissue engineering scaffolds using 3D projection stereolithography. *Biomaterials* **33**, 3824–3834 (2012).
52. W. Hynes, N. J. Doty, T. I. Zarembinski, M. P. Schwartz, M. W. Toepke, W. L. Murphy, S. K. Atzet, R. Clark, J. A. Melendez, N. C. Cady, Micropatterning of 3D microenvironments for living biosensor applications. *Biosensors* **4**, 28–44 (2014).
53. Z. Q. Li, J. Torgersen, A. Ajami, S. Mühleder, X. Qin, W. Husinsky, W. Holnthoner, A. Ovsianikov, J. Stampfl, R. Liska, Initiation efficiency and cytotoxicity of novel water-soluble

two-photon photoinitiators for direct 3D microfabrication of hydrogels. *RSC Adv.* **3**, 15939–15946 (2013).
54. J. Torgersen, A. Ovsianikov, V. Mironov, N. Pucher, X. Qin, Z. Li, K. Cicha, T. Machacek, R. Liska, V. Jantsch, J. Stampfl, Photo-sensitive hydrogels for three-dimensional laser microfabrication in the presence of whole organisms. *J. Biomed. Opt.* **17**, 105008 (2012).
55. Y. Lu, G. Mapili, G. Suhali, S. Chen, K. Roy, A digital micro-mirror device-based system for the microfabrication of complex, spatially patterned tissue engineering scaffolds. *J. Biomed. Mater. Res. A* **77A**, 396–405 (2006).
56. Q. Liang, L. Zhang, Y. Xiong, Q. Wu, H. Tang, A facile method to prepare a polyethylene glycol modified polysilane as a waterborne photoinitiator. *J. Photochem. Photobiol. A Chem.* **299**, 9–17 (2015).
57. D. K. Balta, N. Arsu, Host/guest complex of β-cyclodextrin/5-thia pentacene-14-one for photoinitiated polymerization of acrylamide in water. *J. Photochem. Photobiol. A Chem.* **200**, 377–380 (2008).
58. G. Temel, T. Parali, M. Tulu, N. Arsu, Photopolymerization of acrylamide with benzophenone/methylated-β-cyclodextrin inclusion complex in the presence of jeffamine based dendrimers as coinitiators in aqueous media. *J. Photochem. Photobiol. A Chem.* **213**, 46–51 (2010).
59. D. K. Balta, G. Temel, M. Aydin, N. Arsu, Thioxanthone based water-soluble photoinitiators for acrylamide photopolymerization. *Eur. Polym. J.* **46**, 1374–1379 (2010).
60. G. Temel, N. Arsu, One-pot synthesis of water-soluble polymeric photoinitiator via thioxanthonation and sulfonation process. *J. Photochem. Photobiol. A Chem.* **202**, 63–66 (2009).
61. M. A. Tasdelen, B. Karagoz, N. Bicak, Y. Yagci, Phenacylpyridinium oxalate as a novel water-soluble photoinitiator for free radical polymerization. *Polym. Bull.* **59**, 759–766 (2008).
62. Y. Wang, X. Jiang, J. Yin, A water-soluble supramolecular-structured photoinitiator between methylated β-cyclodextrin and 2,2-dimethoxy-2-phenylacetophenone. *J. Appl. Polym. Sci.* **105**, 3819–3823 (2007).
63. X. Jiang, W. Wang, H. Xu, J. Yin, Water-compatible dendritic macrophotoinitiator containing thioxanthone. *J. Photochem. Photobiol. A Chem.* **181**, 233–237 (2006).
64. S. K. Ghosh, M. Nazimuddin, B. M. Mandal, Water-soluble triplet radical generators as photoinitiators in inverse emulsion polymerization of acrylamide. *Makromol. Chem. Rapid Commun.* **13**, 583–586 (1992).

Acknowledgments: We acknowledge Y. Kalisman for expertise in and support for cryo-TEM imaging, E. Blayvas for environmental scanning electron microscopy imaging, and V. Uvarov for PXRD measurements performed at The Hebrew University Center for Nanoscience and Nanotechnology, Edmond J. Safra Campus, Jerusalem, Israel. We also thank N. Mokrzecka and S. Vafaei for excellent technical assistance at Nanyang Technological University, Singapore. **Funding:** This work was financially supported by the Israel National Nanotechnology Initiative (Focal Technology Area), NTU (Nanyang Technological University)–HUJI (The Hebrew University of Jerusalem)–BGU (Ben Gurion University of the Negev) Nanomaterials for Energy and Water Management Program under the Campus for Research Excellence and Technological Enterprise (CREATE), which is supported by the National Research Foundation, Prime Minister's Office, Singapore, and the Planning and Budgeting Committee (PBC) of the Council for Higher Education in Israel. A part of this research was also financially supported by the National Research Foundation Competitive Research Programme (grant NRF-CRP10-2012-07). **Author contributions:** S.M., A.A.P., and L.L. conceived the study and cowrote the manuscript. S.M. supervised the project. A.A.P., G.S., and L.L. designed and performed the experiments and collected and analyzed the data. I.C. optimized 3D printing ink and performed 3D printing. J.A.J., S.R.T., and N.-J.C. performed and analyzed the experiments related to hydrogel mechanical and biological characterization. All authors discussed and interpreted the results and were involved in the writing. **Competing interests:** The authors declare that they have no competing interests. **Data and materials availability:** All data needed to evaluate the conclusions in the paper are present in the paper and/or the Supplementary Materials. Additional data related to this paper may be requested from the authors.

Submitted 4 October 2015
Accepted 27 February 2016
Published 1 April 2016
10.1126/sciadv.1501381

Citation: A. A. Pawar, G. Saada, I. Cooperstein, L. Larush, J. A. Jackman, S. R. Tabaei, N.-J. Cho, S. Magdassi, High-performance 3D printing of hydrogels by water-dispersible photoinitiator nanoparticles. *Sci. Adv.* **2**, e1501381 (2016).